260-GBaud Single-Wavelength Coherent Transmission Over 100-km SSMF Based on Novel Arbitrary Waveform Generator and Thin-Film Niobate I/Q Modulator

Sylvain Almonacil, *Member, IEEE*, Haik Mardoyan, *Senior Member, IEEE*, Filipe Jorge, Fabio Pittalà, Mengyue Xu, Benjamin Krueger, Fabrice Blache, Bernadette Duval, Lifeng Chen, Yangjie Yan, Xiaoyan Ye, *Member, IEEE*, Amirhossein Ghazisaeidi, *Member, IEEE*, Sina Rimpf, Yuntao Zhu, Jy Wang, Michel Goix, Ziyang Hu, Margaux Duthoit, Markus Gruen, Xinlun Cai, and Jeremie Renaudier, *Senior Member, IEEE*

(Post-Deadline Paper)

***Abstract*—In this paper, we demonstrate up to 260-GBaud single-wavelength coherent transmission by employing an optical transmitter based on two wide-bandwidth devices: a novel 260-GS/s arbitrary waveform generator with a 10-dB bandwidth of 90-GHz and a thin-film Lithium Niobate I/Q modulator with a 3-dB bandwidth of 110-GHz. We first assess the performance of our high symbol rate transmitter for generating spectrally efficient Nyquist multilevel modulation format signals at symbol rates up to 210-GBaud with >1.4-Tbps achievable information rates and by using linear digital signal processing only. We achieve up to 1.84-Tbps at 185-GBaud using PCS-64QAM, highlighting the linear behavior of our transmitter for high symbol rate Nyquist signaling. We then switch to dual-polarization QPSK coherent transmission and further increase the symbol rate up to 260-GBaud. Without using nonlinear digital-signal-processing nor advanced inter-symbol-interference mitigation techniques, we successfully transmit 260-GBaud QPSK at 800-Gbps net rate over 100-km of standard single mode fiber.**

***Index Terms*—Coherent communications, fiber optics components, optical fiber communication, very high-speed modulation.**

Manuscript received 7 December 2022; revised 7 February 2023 and 29 March 2023; accepted 7 April 2023. Date of publication 26 April 2023; date of current version 27 June 2023. This work was supported by European Commission through H2020 QAMeleon Project under Grant 780354. *(Corresponding author: Sylvain Almonacil.)*

Sylvain Almonacil, Haik Mardoyan, Xiaoyan Ye, Amirhossein Ghazisaeidi, and Jeremie Renaudier are with the Nokia Bell Labs, 91300 Massy, France (e-mail: sylvain.almonacil@nokia-bell-labs.com; haik.mardoyan@nokia-bell-labs.com; xiaoyan.ye@nokia.com; amirhossein.ghazisaeidi@nokia-bell-labs.com; jeremie.renaudier@nokia-bell-labs.com).

Filipe Jorge, Fabrice Blache, Bernadette Duval, and Michel Goix are with the III-V Lab, a joint lab of 'Nokia Bell Labs France', 'Thales Research and Technology' and 'CEA Leti', Campus de Polytechnique 1, avenue Augustin Fresnel, RD128 F-91767 Palaiseau Cedex, France (e-mail: filipe.jorge@3-5lab.fr; fabrice.blache@3-5lab.fr; bernadette.duval@3-5lab.fr; michel.goix@3-5lab.fr).

Fabio Pittalà, Benjamin Krueger, Sina Rimpf, Margaux Duthoit, and Markus Gruen are with the Keysight Technologies GmbH, 71034 Böblingen, Germany (e-mail: fabio.pittala@keysight.com; benjamin.krueger@keysight.com; sina.rimpf@keysight.com; margaux.duthoit@keysight.com; markus.gruen@keysight.com).

Mengyue Xu, Yuntao Zhu, and Jy Wang are with the State Key Laboratory of Optoelectronic Materials and Technologies and School of Electronics and Information Technology, Sun Yat-sen University, Guangzhou 510000, China (e-mail: xumy26@mail2.sysu.edu.cn; zhuyt59@mail.sysu.edu.cn; wangjy369@mail2.sysu.edu.cn).

Xinlun Cai is with the State Key Laboratory of Optoelectronic Materials and Technologies and School of Electronics and Information Technology, Sun Yat-sen University, Guangzhou 510000, China, and also with the Red May Industrial Park, Liobate Technologies Limited, Nanjing, Jiangsu 210003, China (e-mail: caixinlun@liobate.com).

Lifeng Chen, Yangjie Yan, and Ziyang Hu are with the Red May Industrial Park, Liobate Technologies Limited, Nanjing, Jiangsu 210003, China (e-mail: chenlifeng@liobate.com; yanyangjie@liobate.com; huziyang@liobate.com).

Color versions of one or more figures in this article are available at https://doi.org/10.1109/JLT.2023.3269740.

Digital Object Identifier 10.1109/JLT.2023.3269740

I. Introduction

While the demand for more bandwidth increases ceaselessly, increasing the aggregate per-wavelength information rate by leveraging high symbol rate systems is required to keep on reducing the cost-per-bit in optical systems [1]. One of the main trends in the telecom industry is the transition to higher symbol rates through integrated optics to reduce the component count, and power consumption. One key component in advanced high-speed coherent systems is the digital-to-analog converter (DAC) to generate high-speed multi-level signals. Usually based on Silicon-Germanium (SiGe) or Complementary Metal-Oxide Semiconductor (CMOS) [2], increasing the bandwidth above 65-GHz without sacrificing on the resolution and the output swing appears challenging. As a result, going beyond 130-GBaud may require specific digital signal processing techniques or to generate data with more than one DAC per dimension. Another key high-speed component is the Mach-Zehnder modulator (MZM) which can be built with high bandwidth technologies, such as the Plasmonic-Organic Hybrid I/Q modulator paired with silicon photonics platform [3], [4], [5], InP MZM [6] or the thin- film lithium niobate (TFLN) modulators with both a high bandwidth and a low drive voltage specification [7], [8], [9].

In that context, intense research efforts focus on pushing the symbol rates well beyond 200-GBaud. To overcome the limited

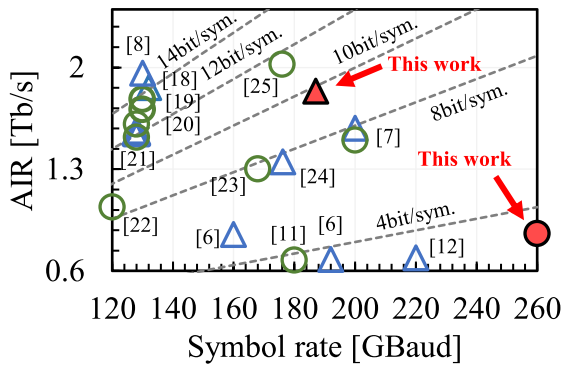

Fig. 1. Reported achievable information rate versus symbol rate above 120-GBaud. Triangles: Back-to-back. Circles: Transmission.

sampling speed and/or analog bandwidth of current DACs, several techniques have been envisioned. In [7], authors use a digital-bandwidth-interleave to multiplex three DACs and thus replicate a 264-GS/s transmitter. By doing so, they demonstrate the transmission of a 200-GBaud multilevel signal. Another technique to combine several DACs is the analog multiplexer (AMUX). In [6], authors report on the generation and detection of a 192-GBaud QPSK signal by using a 2:1 AMUX. In that case, a dedicated DSP at the transmitter is also necessary to benefit from the bandwidth enhancement which comes from this specific type of time-interleaving [10]. Alternatively, authors in [11] reports on the transmission of a 180-GBaud QPSK synthesized by time multiplexing 4x45-Gbps binary streams and cascading 2:1 InP DHBT selectors but without resorting to specific DSP at the transmitter. Finally, prior to this work, the highest reported symbol rate was of 220-GBaud in back-to-back with dual-polarization (DP) QPSK modulation [12]. The transmitter was based on a 256-GSa/s Arbitrary Wavelength Generator (AWG), a >50GHz 6-dB bandwidth gallium arsenide (GaAs) I/Q modulator, nonlinear DSP, and Maximum Likelihood Sequence Estimator (MLSE) to compensate for the highly limited bandwidth of the set-up.

In this work, which builds upon [13], we report, to our best knowledge, the first 260-GBaud DP-QPSK transmission over 100-km of standard single-mode fiber. As a mantra to keep DSP complexity as low as possible, we do not employ nonlinear DSP nor MLSE algorithms. Thus, our result is obtained by leveraging wide bandwidth devices, namely a new 260-GSa/s high-speed AWG, and a TFLN I/Q modulator. The record symbol rate of 260-GBaud exceeds by 30% the previous record without MLSE [7] and by 18% the previous absolute record of 220-GBaud [12] for coherent transmissions. A visual representation of our achievement is shown in Fig. 1, together with recent experimental results of >120-GBaud coherent transmissions.

The rest of the paper is organized as follows. In Section II, we present the experimental set-up and the employed DSP. In Section III, we report the experimental results for multilevel modulation formats and for QPSK up to 260-GBaud. Finally, we draw our conclusions in Section IV.

II. Experimental Set-Up

The Fig. 2(a) shows a schematic of the set-up used for the experiment. The light from an external cavity laser at $\lambda = 1559.77$-nm is coupled to and from the I/Q modulator using edge coupler with a lensed fiber and polarization maintaining fibers. The laser output power is kept constant at 18-dBm. In the next sub-sections, we detail the main components of this optical transmission set-up and of the DSP.

A. Arbitrary Waveform Generator

As a signal source, we employ a prototype of the upcoming Keysight M8199B arbitrary waveform generator to generate I and Q signals. The Fig. 3(a) shows an internal view of the prototype. The main board hosts four 8-bit (physical resolution) SiGe DACs which are 2:1 time interleaved to generate the high frequency output signal. While passive power combiners added up the signals in the predecessor M8199A, an active combiner integrated circuit is used to sum up the signals in the M8199B. Integrated with a linear high-power radio frequency (RF) amplifier in a single gold-brick package, this configuration improves both the output power and the analogue bandwidth. As a result, the AWG features a low-frequency differential output amplitude of >4.5-Vpp and a 10-dB bandwidth of about 90-GHz. The frequency response of the M8199B and its predecessor the M8199A are shown in Fig. 3(b), clearly showing a significant improvement in terms of bandwidth (30%) and in output power (∼6-dB). Also, the smoother decay of the M8199B transfer function with respect to its predecessor enables to perform efficient pre-emphasis of the generated signals beyond 100-GHz, as demonstrated in this work. In Fig. 3(c), we also report the effective resolution (*Effective Number of Bits*, ENoB) of the M8199B both for single-ended and differential output modes. For frequencies smaller than 65-GHz the ENoB is of approximately 6 bits while it reduces to 5-bits above this frequency. Overall, the ENoB values above 5-bits make the AWG compliant for the generation of multilevel spectrally efficient Nyquist signals [14]. Also, the M8199B has a memory length of 2^{20} samples for each analog output. In this work, single-ended output mode is used, and the AWG sampling frequency has been overclocked to 260-GS/s.

B. Transmitter DSP

The digital traces loaded into the M8199B memory are offline generated at 2 samples per symbol before being resampled to match the target symbol rate up to 260-GBaud and finally uniformly quantized over 8 bits. The loaded data consist in 32768-long random symbol sequences mapped on QPSK, 16QAM, 32QAM and PCS-64QAM modulations formats. For operations above 1 sample per symbol, standard Nyquist pulse-shaping is used, i.e., root-raised-cosine pulses with roll-off factor 0.01. At 1 sample-per-symbol, the generated symbols are directly mapped to the corresponding AWG quantization levels. The skew between the I/Q outputs of the AWG are compensated in the analog domain with adjustable delay lines with 30-fs resolution integrated inside the AWG. In this experiment, to compensate

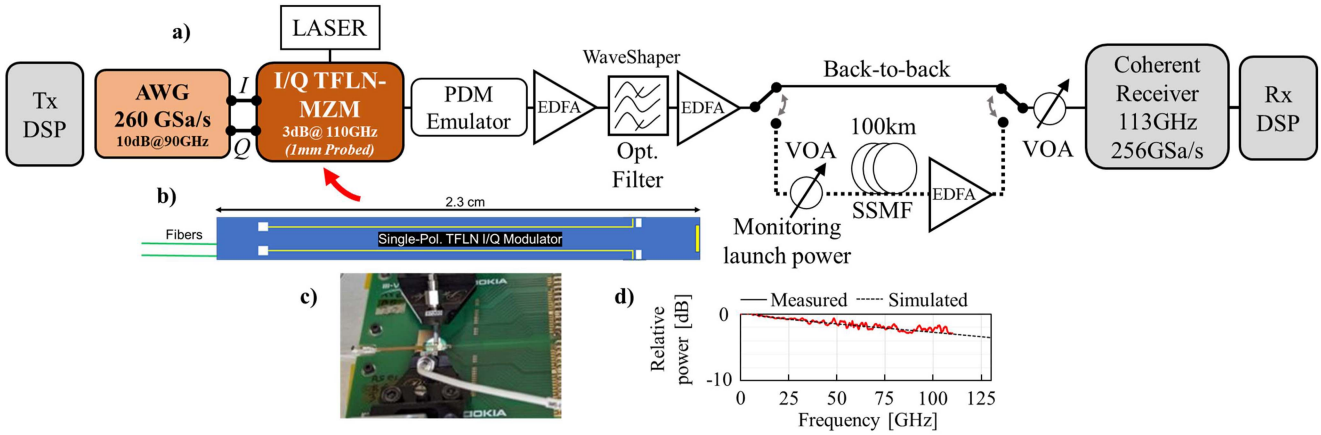

Fig. 2. (a) Experimental set-up. (b) Diagram of the integrated thin-film lithium niobate modulator. (c) Picture of the PCB supporting the TFLN modulator with RF probes. (d) Measured and simulated power transfer function of the TFLN modulator.

the decaying AWG frequency response at high frequencies, we perform optical pre-emphasis only to avoid extra-penalty arising from increased peak-to-average power ratio during electrical signal synthesis. Fig. 4 shows the measured frequency responses of the optical spectrum before and after zero-forcing based optical pre-emphasis.

C. Thin-Film Modulator

The Fig. 2(b) shows a diagram of the used integrated TFLN I/Q modulator based on the TFLN platform in dual-drive push-pull mode. To generate the high symbol rates signals, we operated with high-frequency RF probes for the signal applied to the inputs of the TFLN I/Q modulator. This TFLN I/Q modulator adopts a similar design of traveling-wave electrodes (TWE) and components as in [8], [9]. Edge couplers based on bi-layer inverse taper were used for polarization-insensitive off-chip coupling. The coupling efficiency between the edge coupler and a lensed fiber is less than 4.9-dB/facet. The total fiber-chip-fiber loss is 12.9-dB, including an on-chip loss of ∼3-dB. Note that, for a more flexible RF input layout, we utilize air-bridge structures in the 90-degree bends of the TWE to suppress RF wavefront distortion, leading to a low RF return loss of $<$ -15-dB. All the 23-mm-long sub-MZMs exhibit a half-wave voltage of 1-V and an extinction ratio of at least 35-dB. Our device presents outstanding bandwidth-voltage performance owing to the low RF attenuation of 0.21-dB.cm^{-1}.GHz$^{-1/2}$ of capacitive-loaded-TWE and perfect RF-optical velocity matching. The TFLN I/Q modulator was mounted on a PCB as shown in Fig. 2(c). The high frequency electrical signals from the AWG are set to 1-V peak-to-peak output voltage and directly sent to the modulator inputs through RF probes having an electrical bandwidth greater than 100-GHz. The measured 3-dB electro-optic bandwidth of the demonstrated I/Q modulator achieves 110-GHz, as shown in the measured power transfer function of Fig. 2(d).

D. Transmission

At the modulator output, polarization division multiplexing (PDM) is emulated with a split-and-delay architecture made of free-space optics. The delay between the two polarizations is 10-ns. The dual-polarization output signal is measured at -15dBm and amplified by an Erbium-doped fiber amplifier (EDFA) before applying optical pre-emphasis as described in Section B. The output signal is then launched either directly to the coherent receiver (back-to-back) or to a 100-km SSMF fiber spool with 22-dB loss. At the span entrance, a variable optical attenuator (VOA) enables launched power tuning. Before the optical receiver, the optical signal-to-noise ratio (measured in 0.1-nm bandwidth) is about 39-dB at 260-GBaud.

E. Digital Coherent Receiver and DSP

The digital coherent receiver is made of a VOA, a coherent mixer, a local oscillator, and four commercially available 100-GHz bandwidth balanced Finisar BPDV4121R photodiodes [15] followed by a Keysight Infiniium real-time Digital Storage Oscilloscope with 113-GHz bandwidth and operating at 256-GS/s. Even though the oscilloscope strictly provides less than 1 sample per symbol sampling for the 260-GBaud acquisitions, the 113-GHz brick wall frequency response of the oscilloscope ensures anti-aliasing filtering of the incoming signal. For each measurement, 10 acquisitions of 4 million samples are stored and offline processed. As highlighted previously, we only target mitigation of linear impairments and we do not complement the standard DSP chain with sequence estimators/detectors to mitigate residual inter-symbol interference after data demodulation. The entire DSP flow consists in resampling at 2 samples per symbol, chromatic dispersion compensation (in the transmission case), polarization demultiplexing, carrier frequency estimation, carrier phase estimation and least-mean-square blind equalization to mitigate residual transmitter I/Q imbalances. Blind polarization demultiplexing is performed by the constant modulus algorithm (CMA) for QPSK, 16QAM and 32QAM signals. In the case of PCS-64QAM, we use a dual-stage pilot-assisted equalization approach. A first preliminary CMA is applied, followed by a multi-modulus algorithm (MMA) for fine convergence. The latter periodically uses known QPSK pilots to compute the error functions. The amount of QPSK pilots is

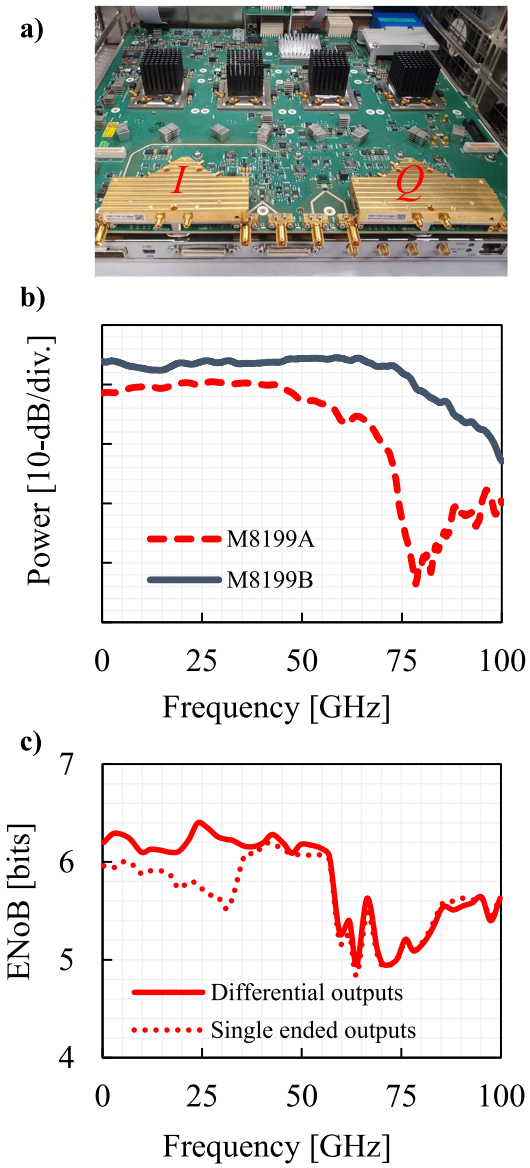

Fig. 3. (a) Inside view of the dual-channel keysight 260-GS/s M8199B arbitrary waveform generator prototype. (b) Frequency responses of the M8199A and of the M8199B. (c) Effective resolution of the M8199B in differential (solid line) or single-ended (dotted line). Output modes.

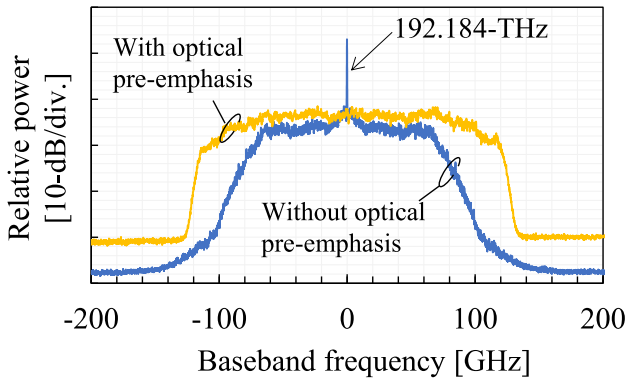

Fig. 4. Optical power spectral density as measured by a WaveAnalyzer 1500s without and with optical pre-emphasis in back-to-back configuration.

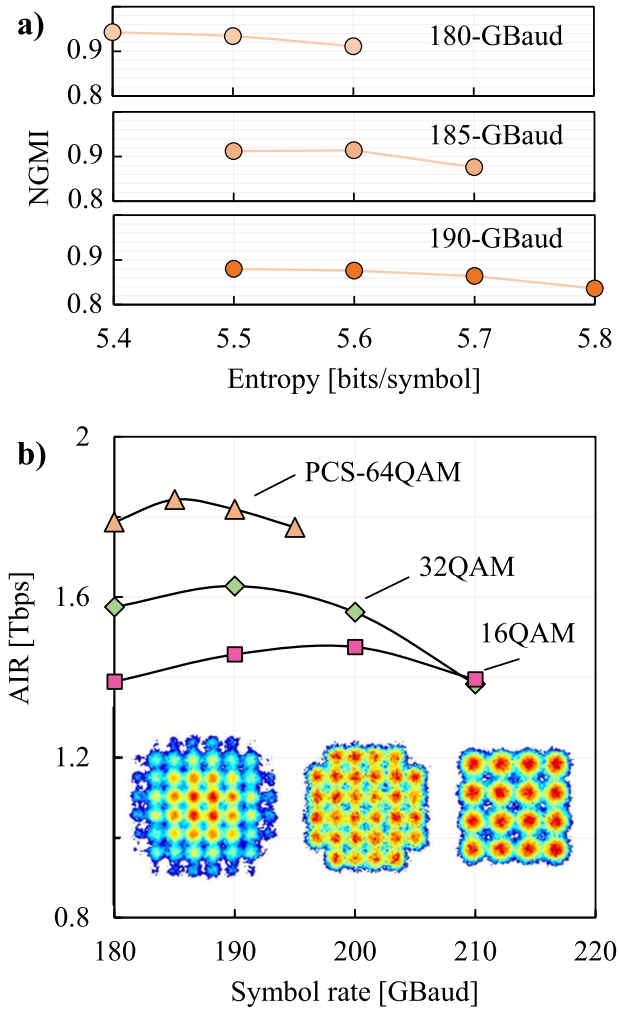

Fig. 5. Experimental results for the multilevel modulation formats. (a) NGMI versus entropy of the PCS-64QAM. (b) Achievable information rate in back-to-back with multilevel modulation formats at >180-GBaud and example of recovered constellations.

2%. More details about this procedure can be found in [16]. The adaptive equalizer used for polarization demultiplexing has a maximum of 221-taps (at 2 samples per symbol), shorter than the polarization decorrelation delay, thereby preventing experimental artifacts. For carrier phase estimation, we employ maximum-likelihood blind-phase search. Finally, we measure the SNR as well as the normalized generalized mutual information (NGMI) to assess the achievable information rate (AIR), corrected from the pilot overhead, if applicable. The number of symbols used for computation of the SNR, NGMI and AIR is about 4 million symbols per data set for the different symbol rates in this experiment.

III. Experimental Results

A. Multilevel Modulation Formats

The back-to-back experimental results with the multilevel modulation formats are reported in Fig. 5. We first report in Fig. 5(a) the NGMI for different entropies of the PCS-64QAM

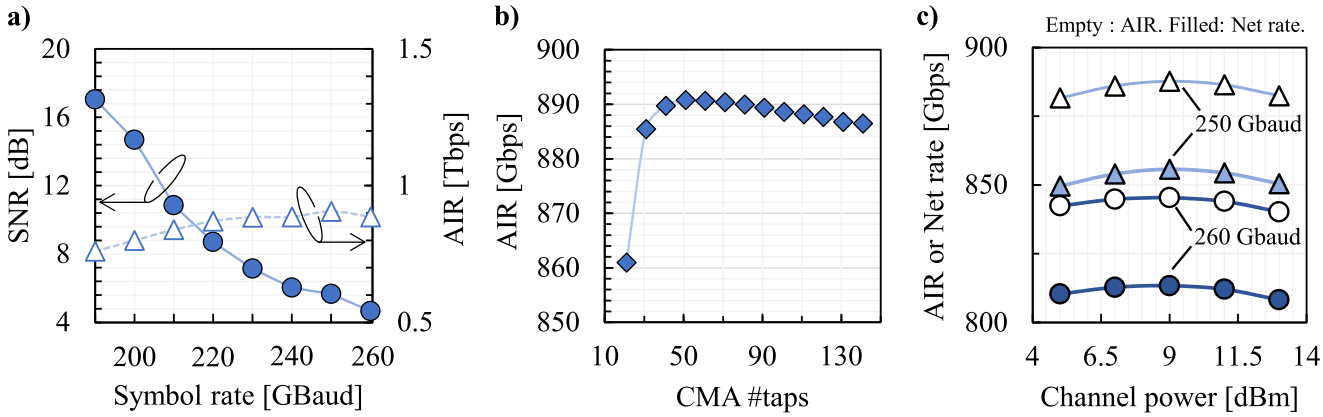

Fig. 6. Back-to-back. (a) Measured SNR and AIR for >190-GBaud DP-QPSK. (b) AIR at 260-GBaud versus constant modulus equalizer number of taps; transmission. (c) 100-km SSMF transmission results.

and for different symbol rates. We observe that for each symbol rate, the NGMI steadily decreases when the signal entropy increases. Also, for each entropy value, the NGMI decreases as the symbol rate increases, owing to the limited bandwidth of the transmitter. Then, we compute the AIR from the NGMI by accounting for a 2% pilot overhead for PCS-64QAM using the formula:

$$AIR = 2 \cdot R \cdot (1 - OH_p) \cdot (H - (1 - NGMI) \cdot m) \quad (1)$$

Where R is the symbol rate, OH_p the pilot overhead (2%), H the PCS signal entropy and m the number of bits per symbol of the square base modulation format (64-QAM, $m = 6$). The maximum AIR is achieved with the PCS-64QAM as shown in Fig. 5(b). The optimal entropy for each symbol rate is found to be respectively 5.5, 5.6, 5.7 and 5.5 bits/symb/pol at 180, 185, 190 and 195-GBaud, respectively. We also report the measured AIR for 16QAM and 32QAM up to 210-GBaud. The maximum measured AIR is 1.63-Tbps with 32QAM and 1.48-Tbps with 16QAM at 190 and 200-GBaud, respectively. For each modulation format, we also represent the DSP output constellation diagrams at the maximum AIR. Overall, we obtain a highest AIR of 1.84-Tbps with 185-GBaud PCS-64QAM and 5.6-bits/symb/pol entropy with an NGMI = 0.914. Regarding the absolute net rates reported recently in the literature at 130-GBaud [8] and at 176-GBaud [25], we approach them by 6% and 9%, respectively. However, nonlinear equalizers at the transmitter and/or receiver were used to push the SNR in both experiments, while our work relies only on linear equalization, confirming the good linear behavior of the AWG at high output swings.

B. Record Symbol Rate With QPSK

For higher symbol-rate experiments, we switch to DP-QPSK format and gradually increase the symbol rate from 190 to 260-GBaud, the highest possible value for a signal at 1 sample-per-symbol with the overclocked 260-GSa/s AWG. We first assess the performance in back-to-back. The measured SNR versus symbol rate between 190 and 260-GBaud is reported in Fig. 6(a). While the SNR is 17-dB at 190-GBaud, it continuously decreases down to 4.7-dB at 260-Gbaud. This decrease results from the increasing fraction of the signal spectrum that undergoes attenuation because of both the limited transfer function of the transmitter, which is not pre-compensated by the WaveShaper above 100-GHz baseband frequency, and of the brick wall frequency response of the ADC cutting-off the signal spectrum above 113-GHz. We also show in Fig. 6(a) the measured AIR above 800-Gbps which is achieved for symbol rates between 200 and 260-GBaud. The maximum AIR is 905-Gbps and is achieved for 250-GBaud.

We show in Fig. 6(b) the measured AIR for the 260-GBaud DP-QPSK in back-to-back as a function of the CMA adaptive equalizer number of taps. We observe that the maximum AIR is achieved with 51-taps. More interestingly, it is possible to lower the number of taps down to 31 with only 5-Gbps of AIR penalty (less than 0.6% over the maximum of 890-Gbps). Thus, owing to the wide bandwidth of the transmitter and receiver, it is possible to transmit the 260-GBaud DP-QPSK signal with an affordable adaptive equalization complexity. We note that a better SNR would be achieved with a DSP strategy like in [17], for instance by targeting 9QAM (duobinary version of QPSK) and solving the residual inter-symbol-interference with a sequence estimator/detector [12]. However, this would lead to an increase in DSP complexity which falls outside the scope of this work.

Finally, we transmitted the 250 and 260-GBaud DP-QPSK signals over 100-km of SSMF while varying launched power. After DSP, all DP-QPSK data were decoded using 18 members of a family of SC-LDPC codes [16] with rates between 0.75 and 0.92 by steps of 0.01. For each data set, the maximum rate resulting in error free FEC decoding is found. We report in Fig. 6(c) the AIR and net ret after FEC decoding as a function of the launched power. Owing to the influence of the back-to-back performance on the overall SNR for such propagation distance, we observe that the 250-GBaud QPSK signal still slightly outperforms over 260-GBaud. However, both signals show successful transmission with net data rates above 800-Gb/s over 100-km SSMF.

IV. Conclusion

We reported on the transmission of up to 260-GBaud dual-polarization (DP) signals without resorting on sequence detection algorithms. This result is obtained by leveraging devices with wide bandwidth, namely a 260-GSa/s arbitrary waveform generator and a TFLN I/Q modulator. We transmitted Nyquist shaped DP signals with high cardinality constellations such as 16QAM, 32QAM and PCS-64QAM from 180 to 210-GBaud. We demonstrated 1.84-Tb/s AIR at 185-GBaud using PCS-64QAM, indicating that >2-Tb/s class signals may become a reality while keeping reasonable DSP complexity. We then transmitted DP-QPSK signals with symbol rate varying from 190 to 260-GBaud and demonstrated error free operation at up to 260-GBaud over 100-km of SSMF, with a net bit rate higher than 800-Gb/s. This is a first step towards single wavelength ultra-long haul 800G DP-QPSK optical transport in future optical networks.

References

[1] "Cisco annual internet report (2018–2023)," 2020. Accessed: Oct. 5, 2023. [Online]. Available: https://www.cisco.com/c/en/us/solutions/collateral/executive-perspectives/annual-internet-report/white-paper-c11-741490.pdf

[2] T. Drenski and J. C. Rasmussen, "ADC & DAC-technology trends and steps to overcome current limitations," in *Proc. Opt. Fiber Commun. Conf. Expo.*, 2018, pp. 1–3.

[3] W. Heni et al., "Ultra-high-speed 2:1 digital selector and plasmonic modulator IM/DD transmitter operating at 222 GBaud for intra-datacenter applications," *J. Lightw. Technol.*, vol. 38, no. 9, pp. 2734–2739, May 2020, doi: 10.1109/JLT.2020.2972637.

[4] Q. Hu et al., "Plasmonic-MZM-based short-reach transmission up to 10 km supporting >304 GBd polybinary or 432 Gbit/s PAM-8 signaling," in *Proc. IEEE Eur. Conf. Opt. Commun.*, 2021, pp. 1–4, doi: 10.1109/ECOC52684.2021.9606060.

[5] H. Mardoyan et al., "Generation and transmission of 160-GBaud QPSK coherent signals using a dual-drive plasmonic-organic hybrid I/Q modulator on silicon photonics," in *Proc. Opt. Fiber Commun. Conf. Exhib.*, 2022, pp. 1–3.

[6] M. Nakamura et al., "192-GBaud signal generation using ultra-broadband optical frontend module integrated with bandwidth multiplexing function," in *Proc. Opt. Fiber Commun. Conf. Exhib.*, 2019, pp. 1–3.

[7] X. Chen et al., "Transmission of 200-GBaud PDM probabilistically shaped 64-QAM signals modulated via a 100-GHz thin-film $LiNbO_3$ I/Q modulator," in *Proc. Opt. Fiber Commun. Conf. Exhib.*, 2021, pp. 1–3.

[8] M. Xu et al., "Dual-polarization thin-film lithium niobate in-phase quadrature modulators for terabit-per-second transmission," *Optica*, vol. 9, pp. 61–62, 2022, doi: 10.1364/OPTICA.449691.

[9] M. Xu et al., "Thin-film lithium niobate DP-IQ modulator for driverless 130 GBaud 64 QAM transmission," in *Proc. Opt. Fiber Commun. Conf. Exhib.*, 2022, Paper Th1J .2.

[10] H. Yamazaki et al., "Digital-preprocessed analog-multiplexed DAC for ultrawideband multilevel transmitter," *J. Lightw. Technol.*, vol. 34, no. 7, pp. 1579–1584, Apr. 2016, doi: 10.1109/JLT.2015.2508040.

[11] G. Raybon et al., "180-GBaud all-ETDM single-carrier polarization multiplexed QPSK transmission over 4480 km," in *Proc. Opt. Fiber Commun. Conf. Exhib.*, 2018, Paper Th4C.3, doi: 10.1364/OFC.2018.Th4C.3.

[12] F. Pittalà, "220 GBaud signal generation enabled by a two-channel 256 GSa/s arbitrary waveform generator and advanced DSP," in *Proc. IEEE Eur. Conf. Opt. Commun.*, 2020, pp. 1–4, doi: 10.1109/ECOC48923.2020.9333130.

[13] H. Mardoyan et al., "First 260-GBd single-carrier coherent transmission over 100 km distance based on novel arbitrary waveform generator and thin-film lithium niobate I/Q modulator," in *Proc. Eur. Conf. Opt. Commun.*, 2022, Paper Th3C.2.

[14] S. Varughese, J. Langston, V. A. Thomas, S. Tibuleac, and S. E. Ralph, "Frequency dependent ENoB requirements for M-QAM optical links: An analysis using an improved digital to analog converter model," *J. Lightw. Technol.*, vol. 36, no. 18, pp. 4082–4089, Sep. 2018, doi: 10.1109/JLT.2018.2859637.

[15] Coherent Corp., "100 GHz balanced photodetector BPDV412xRv," datasheet. Accessed: Mar. 10, 2023. [Online]. Available: https://ii-vi.com/product/100-ghz-ultra-high-speed-balanced-photodetector/

[16] A. Ghazisaeidi et al., "Advanced C+L-band transoceanic transmission systems based on probabilistically shaped PDM-64QAM," *J. Lightw. Technol.*, vol. 35, no. 7, pp. 1291–1299, Apr. 2017, doi: 10.1109/JLT.2017.2657329.

[17] J. M. Estarán et al., "Sub-baudrate sampling at DAC and ADC: Toward 200G per lane IM/DD systems," *J. Lightw. Technol.*, vol. 37, no. 6, pp. 1536–1542, Mar. 2019, doi: 10.1109/JLT.2018.2880690.

[18] M. Nakamura, T. Kobayashi, F. Hamaoka, and Y. Miyamoto, "High information rate of 128-GBaud 1.8-Tb/s and 64-GBaud 1.03-Tb/s signal generation and detection using frequency-domain 8×2 MIMO equalization," in *Proc. IEEE Opt. Fiber Commun. Conf. Exhib.*, 2022, pp. 1–3.

[19] F. Pittalà et al., "1.71 Tb/s single-channel and 56.51 Tb/s DWDM transmission over 96.5 km field-deployed SSMF," *IEEE Photon. Technol. Lett.*, vol. 34, no. 3, pp. 157–160, Feb. 2022, doi: 10.1109/LPT.2022.3142538.

[20] V. Bajaj, F. Buchali, M. Chagnon, S. Wahls, and V. Aref, "Single-channel 1.61 Tb/s optical coherent transmission enabled by neural network-based digital pre-distortion," in *Proc. IEEE Eur. Conf. Opt. Commun.*, 2020, pp. 1–4, doi: 10.1109/ECOC48923.2020.9333267.

[21] F. Buchali et al., "1.52 Tb/s single carrier transmission supported by a 128 GSa/s SiGe DAC," in *Proc. Opt. Fiber Commun. Conf. Exhib.*, 2020, pp. 1–3.

[22] M. Nakamura et al., "1.04 Tbps/carrier probabilistically shaped PDM-64QAM WDM transmission over 240 km based on electrical spectrum synthesis," in *Proc. Opt. Fiber Commun. Conf. Exhib.*, 2019, pp. 1–3.

[23] M. Nakamura et al., "1.3-Tbps/carrier net-rate signal transmission with 168-GBaud PDM PS-64QAM using analogue-multiplexer-integrated optical frontend module," in *Proc. IEEE Eur. Conf. Opt. Commun.*, 2019, pp. 1–3, doi: 10.1049/cp.2019.0845.

[24] X. Chen et al., "Generation and intradyne detection of single-wavelength 1.61-Tb/s using an all-electronic digital band interleaved transmitter," in *Proc. Opt. Fiber Commun. Conf. Expo.*, 2018, pp. 1–3.

[25] M. Nakamura et al., "Over 2-Tb/s net bitrate single-carrier transmission based on >130-GHz-bandwidth InP-DHBT baseband amplifier module," in *Proc. Eur. Conf. Opt. Commun.*, 2022, pp. 1–4.